Variant ATRX syndrome with dysfunction of *ATRX* and *MAGT1* genes

Ying Qiao,[1,2]* Kajari Mondal,[3]* Valentina Trapani, [4]* Jiadi Wen,[1] Gillian Carpenter,[5] Robert Wildin,[6] E. Magda Price,[2,7,8] Richard J. Gibbons R, [9] Jennifer Eichmeyer,[6] Ruby Jiang,[7] Barbara DuPont,[10] Sally Martell,[1] Suzanne M. E. Lewis,[2] Wendy P. Robinson,[2,7] Mark O'Driscoll,[5] Federica I. Wolf, [4 #] Michael E. Zwick,[3 #] Evica Rajcan-Separovic[1#]

*co-first authors

co-corresponding authors

1. Department of Pathology, University of British Columbia (UBC), Vancouver, BC, Canada
2. Department of Medical Genetics, UBC, Vancouver, BC, Canada
3. Department of Human Genetics, Emory University, Atlanta, USA
4. Istituto di Patologia Generale, Università Cattolica del Sacro Cuore, Rome, Italy
5. Human DNA Damage Response Disorders Group, Genome Damage & Stability Centre University of Sussex, UK
6. St Lukes Hospital, Boise, Idaho, USA
7. Child and Family Research Institute, 950 West 28th Avenue, Vancouver, BC, Canada
8. Department of Obstetrics and Gynaecology, UBC, Vancouver, BC, Canada
9. MRC Molecular Hematology Unit, John Radcliffe Hospital, Oxford, UK
10. Greenwood Genetic Center, Greenwood, South Carolina, USA

Corresponding authors:

Dr. Evica Rajcan-Separovic
Department of Pathology (Cytogenetics)
BC Child and Family Research Institute
University of British Columbia
950 West 28th Avenue, Room 3060

Vancouver, BC V5Z 4H4, Canada
Phone: 604-875-3121
Fax: 604-875-3601
Email: eseparovic@cw.bc.ca

Dr. Michael E. Zwick
Department of Human Genetics,
Whitehead Biomedical Research Building
615 Michael St., Suite 301
Emory University, Atlanta, GA 30322, USA
Phone: 404-727-9924
Email: mzwick@emory.edu

Dr. Federica I. Wolf
Istituto di Patologia Generale,
Università Cattolica del Sacro Cuore,
Facoltà di Medicina "A. Gemelli"
Largo F. Vito, 1
00168 – Roma Rome, Italy
Email: federica.wolf@rm.unicatt.it

ABSTRACT

A 0.8kb intronic duplication in *MAGT1* and a single base pair deletion in the last exon of *ATRX* were identified using a chromosome X specific microarray and exome sequencing in a family with 5 males demonstrating intellectual disability (ID) and unusual skin findings (e.g. generalized pruritus). MAGT1 is a Mg^{2+} transporter previously associated with primary immunodeficiency and ID, while mutations in *ATRX* cause ATRX-ID syndrome. In patient cells, the function of ATRX was demonstrated to be abnormal based on altered RNA/protein expression, hypomethylation of rDNA, and abnormal cytokinesis. Dysfunction of MAGT1 was reflected in reduced RNA/protein expression and Mg^{2+} influx. The mutation in *ATRX* most likely explains the ID, while *MAGT1* disruption could be linked to abnormal skin findings, as normal magnesium homeostasis is necessary for skin health. This work supports observations that multiple mutations collectively contribute to the phenotypic variability of syndromic ID, and emphasizes the importance of correlating clinical phenotype with genomic and cell function analyses.

Key words: ATRX, MAGT1, intellectual disability (ID), copy number variants (CNVs), exome, chromosome X

X-linked forms of intellectual disability (ID) are suspected in families with multiple affected males and account for 10% of ID cases. It is estimated that when mutated, ~150-200 genes on the X chromosome can cause X-linked ID (XLID, previously X-linked Mental Retardation-XLMR) [Lubs et al., 2012]. High resolution chromosome arrays and exome sequencing expand the number of potentially pathogenic variants in X-linked neurocognitive disorders (ID and/or autism spectrum disorders (ASD) [Whibley et al., 2010; Nava et al., 2012] and help to dissect the genomic and phenotypic heterogeneity confounding variably presenting ID syndromes [Field et al., 2012].

Using an approach combining targeted high-resolution array analysis and exome sequencing of chromosome X, we report the discovery, as well as clinical and functional correlates, of two novel variants in *ATRX* (OMIM accession number 300032) and *MAGT1* (OMIM accession number 300715) that co-segregate with ID in a large multi-generational family. While mutations at each locus have previously been linked to ID, our data suggest that functional changes at both loci likely underlie the atypical ATRX syndrome presentation in a multi-generational family, including previously undescribed, unusual skin abnormalities.

ATRX belongs to a Snf2 (Sucrose-non-fermenting 2) family of helicase/ATPases, members of which are involved in regulation of transcription, control of cell cycle, DNA repair, and mitotic chromosome segregation [Gibbons and Higgs, 2000]. It is believed that all of these functions are facilitated by chromatin remodeling. Over 100 *ATRX* mutations have been reported to date. Most mutations are located in the N-terminal (zinc finger motif) ADD domain (~50%) and central helicase domain (~30%), while fewer mutations are seen in the more conserved C terminal end [Gibbons and Higgs, 2000], which consists of P and Q boxes possibly involved in transcriptional regulation and protein-protein interaction, respectively. The typical phenotypic features of ATRX syndrome affect ~90% of cases and include severe ID, typical dysmorphic facial features, and skeletal abnormalities. Other common features of ATRX syndrome (>50%

cases) include microcephaly, neonatal hypotonia, genital abnormalities, gut dysmotility, and short stature. HbH inclusions are also common (>87% of cases) and are due to the precipitation of extra beta globin chains caused by aberrant regulation of alpha globin expression by mutated *ATRX*.

MAGT1 is a plasma membrane Mg^{2+} transporter expressed ubiquitously in human tissues, with particular abundance in epithelial cells [Wolf and Trapani, 2011]. Magnesium is involved in a wide variety of biochemical reactions that modulate key cell functions, such as proliferation, differentiation, migration, and apoptosis. Alterations in magnesium availability by dietary intake have been widely studied in animals and Mg^{2+}-deficient rats display clinical signs of skin inflammation, including pruritus [Makiura et al., 2004]. Genetic changes in *MAGT1* have been reported in a family with XLID [Molinari et al., 2008] and more recently associated with X-linked immunodeficiency [Li et al., 2011]. The later study demonstrated that MAGT1 dysfunction leads to abnormal T cell activation due to abnormal Mg^{2+} influx.

The family in this study was ascertained for ID and dysmorphic features identified in the proband (IV-1), who also had short stature (measuring consistently below the 3rd percentile at 5-6 SD below respective height and weight means), seizures, chronic constipation, pruritus, soft crinkly skin of the palms and soles with excess creasing, and cracked, curved toenails (see clinical details in Supplementary Table 1). Developmentally, IV-1 was non-verbal, with profound cognitive deficit, and also met diagnostic criteria for an Autism Spectrum Disorder (ASD) within the Pervasive Developmental Disorder Not Otherwise Specified domain (PDD-NOS). Brain MRI at age 2 years was normal as well as his genitourinary findings. Laboratory results for immunodeficiency panel (T, B, NK), immunoglobulins (IgA, IgM, IgG), serum magnesium, HbH inclusions and transferrin glycosylation, as well as karyotype and FRAXA trinucleotide repeat length, were all normal. Family history revealed that his two cousins (IV-2 and IV-3), maternal male second cousin (III-3) and maternal great-uncle (II-2) also had ID (see

pedigree in Supplementary Figure 1). Detailed clinical assessment was possible for the cousins of IV-1, while the information on older males was obtained from photographs and relatives (Supplementary Table 1). The features common to all affected males included unusual facies and a range of skin abnormalities. Two male cousins (IV-2 and IV-3) shared round inverted triangular facies, with highly-arched eyebrows, short, down-slanting palpebral fissures, and prominent ears (Supplementary Figure 2). The proband and the cousins also shared severe expressive language delay, cracked, longitudinally-grooved nails, and generalized hypotonia. The skin abnormalities noted in at least 3/5 affected male subjects included pruritus and soft crepe paper-like hyperkeratosis of palms and soles. A range of other skin abnormalities were also detected: crinkly skin, hive like changes, eczema, and mild hyperpigmentation. Cutaneous flushing and marked decrease in sensitivity to temperature and/or pain was also recurrent and seen in 4/5 and 3/5 males, respectively. The carrier females were phenotypically normal, with only minor anomalies consisting of grooved nails in the great-grandmother (I-2) and the proband's mother (III-1), spotty depigmentation of III-1's right forearm (Supplementary Figure 2) and right lower chest together with pruritus. The carrier females did not show subjective evidence of developmental deficit.

The initial whole chromosome microarray analysis of proband IV-1 identified a maternal CNV duplication mapping to Xp22.31 (hg18, ChrX: 6,467,401-8,091,811) and a de novo CNV deletion on 11p15 (hg18, Chr11: 18,994,447-19,849,379). Our initial aim was to explore the clinical significance of the Xp22.31 duplication CNV detected in the proband IV-1, considering its uncertain role in ID [Liu et al., 2011]. QMPSF and/or array analysis (chromosome X specific or whole genome, Supplementary methods) determined that the Xp22.31 CNV was not present in the two cousins, and was transmitted from the phenotypically normal great grandfather I-1 (Supplementary Figure 1, Supplementary Table 2). All tested females had extremely skewed X inactivation (>99%) regardless of whether they carried the Xp22.31 duplication. Taken together

these results indicate that the Xp22.31 CNV is not likely to be associated with ID in this family. The chromosome X specific array of IV-2 and IV-3 revealed a small 0.8kb CNV on Xq21.3, with breakpoints in intron 3 of *MAGT1* (hg18, ChrX: 77,009,644-77,010,488; Supplementary Figure 3). The *MAGT1* CNV mapped to the region including markers AR-CAG repeat, DXS1222 and DXS1217 (minimum haplotype), which was found consistently on the inactive chromosome X in the females and all affected males. The range for the minimal haplotype block was from ChrX: 66,705,408-88,382,862, while a wider haplotype block from the first non-segregating marker was from ~ChrX: 46,319,301-140,000,000 (Supplementary methods). Subsequent chromosome X specific arrays showed that the *MAGT1* CNV was present in the great grandmother (I-2) of the proband and in IV-1 and III-1. This CNV contained an alternative splice site, however reverse transcription PCR products from *MAGT1* cDNA using primers for exon 1 and 5, and 1 and 8 respectively did not demonstrate presence of different isoforms (Supplementary methods and Supplementary Figure 4). The role of the *MAGT1* CNV in causing ID was uncertain based on recent reports that a mutation in *MAGT1* leading to ablation of its function did not cause cognitive dysfunction [Li et al., 2011]. Because the CNV analysis did not identify an obvious causative mutation for the ID in this family, and given the apparent X-linked pattern of inheritance in this family, we performed chromosome-X exome sequencing to determine if other mutations might contribute to the XLID and associated phenotypes observed.

We sequenced the X-chromosome exome in two male ID patients (IV-2 and IV-3) using a custom RainDance Technologies chromosome-X exome library for enrichment followed by Illumina sequencing (Supplementary methods, [Mondal et al., 2011]). The median depth of coverage for the two samples was 505 and 449, with nearly 98% of targeted bases having more than 8X coverage in both IV-2 and IV-3. A total of 1,109 variants (SNVs and indels) were called in the two samples (Supplementary Table 3). After filtering (see Supplementary methods) we followed up 3 exonic variants [*ATRX* (p.G2465Vfs*15), *ATG4A* (p.N234K), *TENM1*

(p.H2185L)]. All three variants were validated with Sanger sequencing in IV-2 and IV-3. Supplementary Table 4 and 5 show the validation outcome and list of primers used for sequencing, respectively while Supplementary Figure 3 shows validation of *ATRX* mutation by Sanger sequencing. *ATRX* and *ATG4A* variants segregated with the phenotype while *TENM1* (OMIM accession number 300588) did not. Further functional assessment of *ATG4A* (OMIM accession number 300663) was not performed due to uncertain association with human disease involving ID (it is a member of the autophagin protein family) and normal mRNA and protein expression (Supplementary Figure 5). The single base pair deletion in ATRX was the most promising variant identified due to its association with ID. The length of the wild type ATRX protein is 2492 amino acids (GenBank:AB102641.1). The novel single base deletion we detected (at NM_000489.4(ATRX_v001):c.7394del) in the *ATRX* gene is found in the last coding exon of *ATRX* and is predicted to result in a frame-shift mutation after 2464 amino acids. The frame-shift leads to 14 novel amino acids downstream of the deletion and ultimately generates a premature stop codon after 2478 amino acids, reducing the protein length by 14 amino acids. No well-known structural domains have been reported in this region, although a low complexity region is predicted from 2467-2480 amino acids. This frame-shift mutation in the *ATRX* gene has not been previously reported, and its functional consequence is uncertain, as it falls near to the C-terminal end of the protein and majority of the protein sequence remains unaffected.

We performed a series of functional assays in patient EBV-transformed lymphoblast cell lines (LCLs) in order to determine which of the two variants in *ATRX* and *MAGT1* are causative of the observed phenotype (Supplementary methods). *ATRX* had increased mRNA and decreased protein expression (Figure 1A-C), while *MAGT1* had decreased RNA and protein expression (Figure 1D-F). Ribosomal (rDNA) methylation (Figure 2A and 2B) was performed to further assess the function of ATRX. It was previously shown [Gibbons et al., 2000] that ATRX binds to the p-arm of acrocentric chromosomes, the genomic location of

repetitive rDNA, and that the average methylation of rDNA promoters was significantly reduced in a set of ATRX patients in comparison to controls. We developed a novel Pyrosequencing assay targeting 26 CpG sites across the rDNA repeat promoter in the same region measured by Gibbons et al [Gibbons et al., 2000]. The rDNA methylation level in four affected individuals (IV-1, IV-2, IV-3, III-3) was significantly reduced (17.6%, SD=4.2%) in comparison to an unrelated control group (mean=30.5%, range 14.7-44.2%, SD=9.9%) (p=0.02), while rDNA methylation in five carriers (III-1, III-2, II-1, II-3, I-2) (21.6%, SD=5.9), did not differ from that of the controls. Average rDNA methylation in an unrelated positive control with clinical features of ATRX was 11.5%, and comparable to the level seen in our affected subjects. Further assessment of ATRX function was performed by evaluating the spontaneous levels of binucleate cells and micronuclei in LCLs from affected males which were both found to be elevated in comparison to controls (Figure 2C and 2D). This is consistent with impaired cytokinesis in keeping with the role of ATRX in chromosome cohesion, segregation as well as progression through mitosis [Ritchie et al., 2008].

Impaired MAGT1 function was demonstrated based on reduced basal Mg^{2+} influx ability in patients' Mag-Fluo-4 loaded LCLs in comparison to controls (Figure 2E and 2F) and Supplementary methods). Mg^{2+} influx in both patients was significantly lower than either controls or carrier, while differences between controls and carrier were not significant using ANOVA followed by Newman-Keuls post-hoc test. Thus, not only do patients have lower MAGT1 expression, but they also display an impaired Mg^{2+} uptake in basal conditions.

Phenotypic variability in established syndromes can be due to variable genetic and environmental factors. The mutation in the *ATRX* gene described in our study occurred in the most distal exon of *ATRX* and to the best of our knowledge represents the most 3' end mutation reported (Supplementary Figure 3). Constitutional mutations in the 3' end of *ATRX* were noted in 6 subjects and were associated with fairly typical ATRX-ID syndrome but with

severe genital abnormalities [Gibbons et al., 2008].

The functional defect of *ATRX* due to the mutation in the last exon found beyond the Q-box is evidenced in our subjects by changes in mRNA and protein expression, reduced methylation of rDNA, and abnormal cytokinesis in comparison to controls. The functional defects of ATRX are the most likely explanation for the developmental delay and facial dysmorphism in the affected males. The occurrence of the mutation at the very terminal end of the gene could explain the lack of common ATRX syndrome related features that are typically associated with mutations in the ADD or helicase segment of the gene [Gibbons and Higgs, 2000].

The skin/nail pathology (pruritus, dyskeratosis, blotchy skin and cracked, grooved nails) is a unique finding in our subjects and has not been previously reported in ATRX syndrome patients. It could be attributed to the disruption of *MAGT1* due to a small duplication. Larger deletions, but not duplications, overlapping the *MAGT1* CNV were reported in the cognitive normal controls from Database of Genomic Variants. The health of these controls is otherwise largely unknown. The orientation of the *MAGT1* duplication (tandem, inverted) or its unique genomic location within the gene could have resulted in reduction in MAGT1 RNA and protein expression and Mg^{2+} influx and consequently impaired the cellular magnesium homeostasis. Magnesium deficiency has been associated with skin pathology in rats fed low Mg^{2+} diet (e.g. scratching, wrinkly skin) [Makiura et al., 2004]. The pain/heat insensitivity noted in younger and older affected males is also of interest in our family considering the role of Mg^{2+} in central nervous system excitability [Durlach et al., 2000].

It is of interest to note the difference between our subjects with *MAGT1* dysfunction and the subjects from two families reported recently by Li et al. [Li et al., 2011], who had normal cognitive development and no skin pathology despite the almost complete loss of MAGT1 protein function due to *MAGT1* mutations (splice donor and nonsense). Absence or significant

reduction of MAGT1 protein without an impact on patients' cognitive function, questions the role of the gene in ID as reported by Molinari et al [Molinari et al., 2008]. The main pathology noted in subjects described by Li et al was impaired T cell function, and immunodeficiency[Li et al., 2011]. In contrast, our subjects did not demonstrate immunodeficiency, with chronic rhinitis in IV-2 and IV-3 being the only sign of potential infection, possibly as the mutation we describe only slightly affects the protein expression levels. T-cells were not available from our patients for functional studies. Furthermore, in our subjects the *MAGT1* intronic duplication could have a tissue specific effect on the isoform that is expressed in skin cells specifically. The reduction in Mg^{2+} influx in our patients could therefore be due either to the reduction in mRNA and protein expression levels or to the malfunction of the mutated protein. An additional difference between the two studies is that we measured the Mg^{2+} influx in B cells that were transformed by EBV, while the findings in the subjects studied by Li et al were obtained in B cells naturally infected by EBV [Li et al., 2011]. In vitro immortalization by EBV does not produce tumorigenic cells, in contrast to natural infection. Therefore, the naturally EBV-infected B cells in patients described by Li et al., [Li et al., 2011] might have acquired several alterations changing the normal cellular control. In B cells from patients studied by Li et al intracellular Mg^{2+} levels were lower, and upon stimulation cell response was normal, however the basal Mg^{2+} influx capacity was not reported. Finally, our cases have an additional mutation in a highly relevant candidate gene *ATRX*, which controls expression of many genes, through chromatin conformation rendering the genetic set up and clinical presentation of our patients different and unique. The presence of two genetic abnormalities in the 500kb region is intriguing and might be a chance event or suggest the region's (or overall) impaired genomic stability or DNA repair.

The clinical presentation of IV-2 and IV-3 was most comparable, possibly due to the fact that they carried only the *ATRX* mutation and *MAGT1* CNV. Proband IV-1, however, had an additional de novo deletion of 11p15 containing 5 genes. Deletions and duplications within this

region were reported in ISCA and Decipher, but the phenotype other than ID or CNV origin was not specified. One of the genes within this CNV was *HIP14* previously reported to mediate Mg^{2+} uptake [Goytain et al., 2008], and it is of interest that IV-1 had a lower Mg^{2+} influx in comparison to his cousin IV-2, although their skin pathology did not differ. It is possible that some of the unique features of proband IV-1 (e.g. different facial features and marked short stature) were due to the 11p15 CNV and its integral genes, including *MRGX2, CSRP3, E2F8* and *NAV2*. Proband IV-1 also had the Xp22.31 duplication transmitted from his phenotypically normal grandfather, however a panel of tests including skewed X inactivation and haplotype analysis excluded the segregation of this CNV with the abnormal phenotype.

Our study provides further support to the phenotypic variability that exists due to multiple genetic defects [Girirajan et al., 2010; O'Roak et al., 2011]. The contribution of the two mutations that segregate with the phenotype in our family was initially ambiguous as the *MAGT1* CNV is in the intron and the *ATRX* mutation is in the region of the gene lacking functional annotation. The change in cellular function in the affected subjects supports their role in the phenotype and helps explain the clinical presentation of ID, including the unique skin pathology. The reported variant in *ATRX* has been submitted in www.lovd.nl/ATRX. The reported CNV variant in *MAGT1* has been entered in DECIPHER (http://decipher.sanger.ac.uk/, CFRI279207).

ACKNOWLEDGMENTS

This work was supported by funding from the Canadian Institutes for Health Research (CIHR) (MOP 74502; PI: ERS). MESL and ERS are Career Scholars supported by the Michael Smith Foundation for Health Research. The authors appreciate the collaboration and support of the participating subjects and their families.

CONFLICT OF INTEREST STATEMENT

We declare no conflict of interest in our manuscript titled as " Variant ATRX syndrome with dysfunction of *ATRX* and *MAGT1* genes".

FIGURE LEGENDS:

Figure 1. ATRX and MAGT1 expression. A) Increase in ATRX RNA expression in comparison to controls; B) Reduced ATRX protein expression in patients C) Western blot for 300kDa band indicating reduction in ATRX protein expression (C1-C3=controls); D) Reduction of MAGT1 RNA expression in patients; E) and F) Reduction of MAGT1 protein expression in patients in comparison to controls. * indicates $P<0.05$. ** indicates $P<0.01$.

Figure 2. ATRX and MAGT1 functional abnormalities. A) Overall rDNA promoter methylation is reduced in patients in comparison to controls; B) This trend is visible across the 26 CpG sites assayed in the rDNA promoter. Error bars represent standard error of the mean within each group (carrier n=5, affected n=4 and negative controls n=25); C) Increased presence of binucleate cells in patients in comparison to controls; D) Increased presence of micronuclei in patients in comparison to controls. E) Mg^{2+} influx is reduced in patients (red and purple) in comparison to controls and carrier female (C=control). F) Fluorescence increments after 15 min from Mg^{2+} addition (arrow) were analyzed by ANOVA (n=3); different letters (a and b) indicate statistically different samples ($P<0.05$, Newman-Keuls post-hoc test).

REFERENCES:

Durlach J, Bac P, Bara M, Guiet-Bara A. 2000. Physiopathology of symptomatic and latent forms of central nervous hyperexcitability due to magnesium deficiency: a current general scheme. Magnes Res 13:293-302.

Field M, Scheffer IE, Gill D, Wilson M, Christie L, Shaw M, Gardner A, Glubb G, Hobson L, Corbett M, Friend K, Willis-Owen S, et al. 2012. Expanding the molecular basis and phenotypic spectrum of X-linked Joubert syndrome associated with OFD1 mutations. Eur J Hum Genet 20:806-9.

Gibbons RJ, Higgs DR. 2000. Molecular-clinical spectrum of the ATR-X syndrome. Am J Med Genet 97:204-12.

Gibbons RJ, McDowell TL, Raman S, O'Rourke DM, Garrick D, Ayyub H, Higgs DR. 2000. Mutations in ATRX, encoding a SWI/SNF-like protein, cause diverse changes in the pattern of DNA methylation. Nat Genet 24:368-71.

Gibbons RJ, Wada T, Fisher CA, Malik N, Mitson MJ, Steensma DP, Fryer A, Goudie DR, Krantz ID, Traeger-Synodinos J. 2008. Mutations in the chromatin-associated protein ATRX. Hum Mutat 29:796-802.

Girirajan S, Rosenfeld JA, Cooper GM, Antonacci F, Siswara P, Itsara A, Vives L, Walsh T, McCarthy SE, Baker C, Mefford HC, Kidd JM, et al. 2010. A recurrent 16p12.1 microdeletion supports a two-hit model for severe developmental delay. Nat Genet 42:203-9.

Goytain A, Hines RM, Quamme GA. 2008. Huntingtin-interacting proteins, HIP14 and HIP14L, mediate dual functions, palmitoyl acyltransferase and Mg2+ transport. J Biol Chem 283:33365-74.

Li FY, Chaigne-Delalande B, Kanellopoulou C, Davis JC, Matthews HF, Douek DC, Cohen JI, Uzel G, Su HC, Lenardo MJ. 2011. Second messenger role for Mg2+ revealed by human T-cell immunodeficiency. Nature 475:471-6.

Liu P, Erez A, Nagamani SC, Bi W, Carvalho CM, Simmons AD, Wiszniewska J, Fang P, Eng PA, Cooper ML, Sutton VR, Roeder ER, et al. 2011. Copy number gain at Xp22.31 includes complex duplication rearrangements and recurrent triplications. Hum Mol Genet 20:1975-88.

Lubs HA, Stevenson RE, Schwartz CE. 2012. Fragile X and X-linked intellectual disability: four decades of discovery. Am J Hum Genet 90:579-90.

Makiura M, Akamatsu H, Akita H, Yagami A, Shimizu Y, Eiro H, Kuramoto M, Suzuki K, Matsunaga K. 2004. Atopic dermatitis-like symptoms in HR-1 hairless mice fed a diet low in magnesium and zinc. J Int Med Res 32:392-9.

Molinari F, Foulquier F, Tarpey PS, Morelle W, Boissel S, Teague J, Edkins S, Futreal PA, Stratton MR, Turner G, Matthijs G, Gecz J, et al. 2008. Oligosaccharyltransferase-subunit mutations in nonsyndromic mental retardation. Am J Hum Genet 82:1150-7.

Mondal K, Shetty AC, Patel V, Cutler DJ, Zwick ME. 2011. Targeted sequencing of the human X chromosome exome. Genomics 98:260-5.

Nava C, Lamari F, Heron D, Mignot C, Rastetter A, Keren B, Cohen D, Faudet A, Bouteiller D, Gilleron M, Jacquette A, Whalen S, et al. 2012. Analysis of the chromosome X exome in patients with autism spectrum disorders identified novel candidate genes, including TMLHE. Transl Psychiatry 2:e179.

O'Roak BJ, Deriziotis P, Lee C, Vives L, Schwartz JJ, Girirajan S, Karakoc E, Mackenzie AP, Ng SB, Baker C, Rieder MJ, Nickerson DA, et al. 2011. Exome sequencing in sporadic autism spectrum disorders identifies severe de novo mutations. Nat Genet 43:585-9.

Ritchie K, Seah C, Moulin J, Isaac C, Dick F, Berube NG. 2008. Loss of ATRX leads to chromosome cohesion and congression defects. J Cell Biol 180:315-24.

Whibley AC, Plagnol V, Tarpey PS, Abidi F, Fullston T, Choma MK, Boucher CA, Shepherd L, Willatt L, Parkin G, Smith R, Futreal PA, et al. 2010. Fine-scale survey of X chromosome copy number variants and indels underlying intellectual disability. Am J Hum Genet 87:173-88.

Wolf FI, Trapani V. 2011. MagT1: a highly specific magnesium channel with important roles beyond cellular magnesium homeostasis. Magnes Res 24:S86-91.

Figure 1

A.

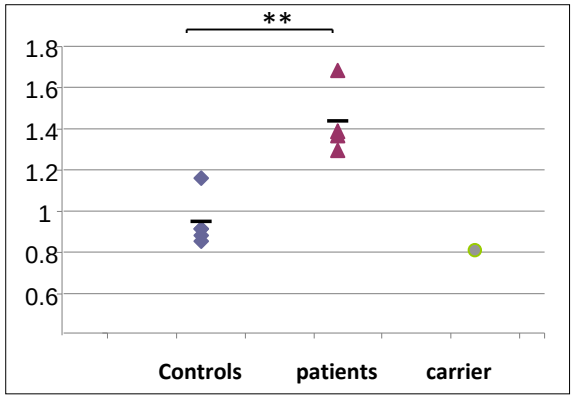

B.

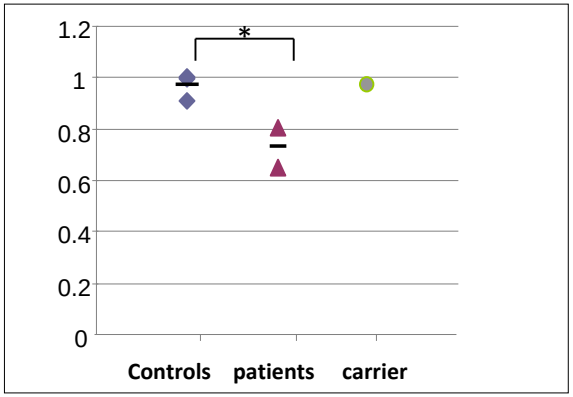

C.

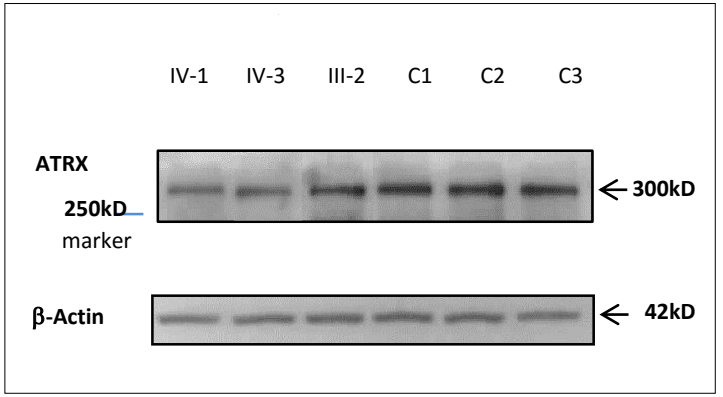

D.

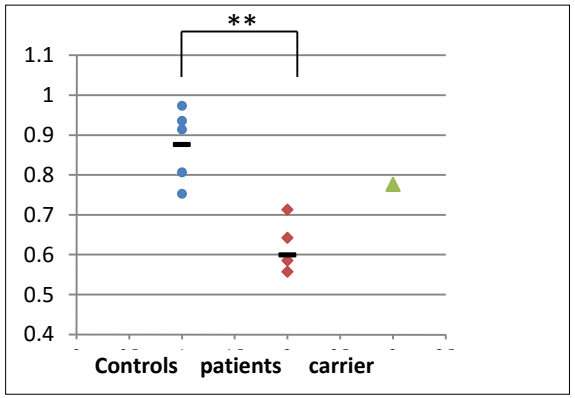

E.

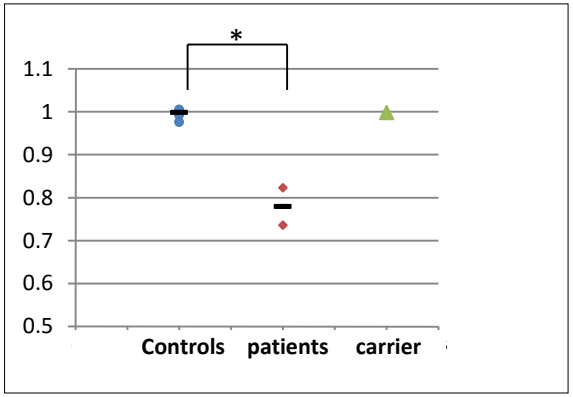

F.

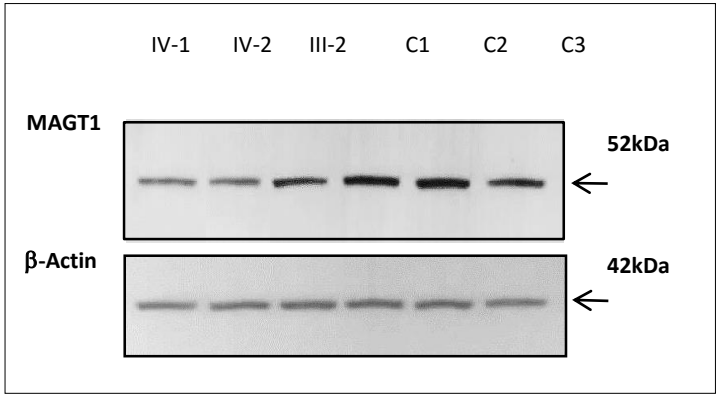

◆ control
▲ patient
● carrier

Figure 2.

A.

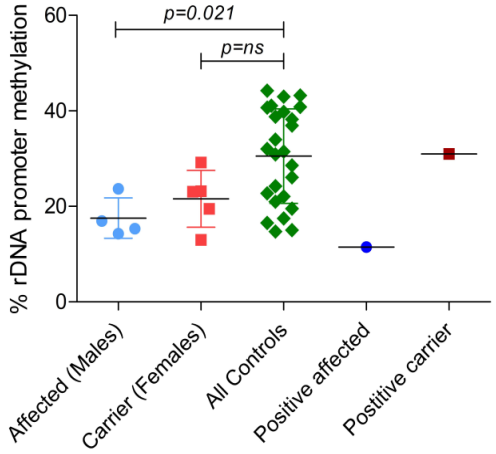

B.

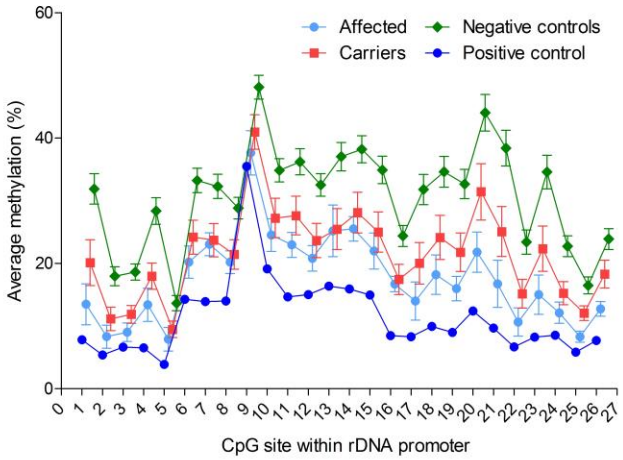

E.

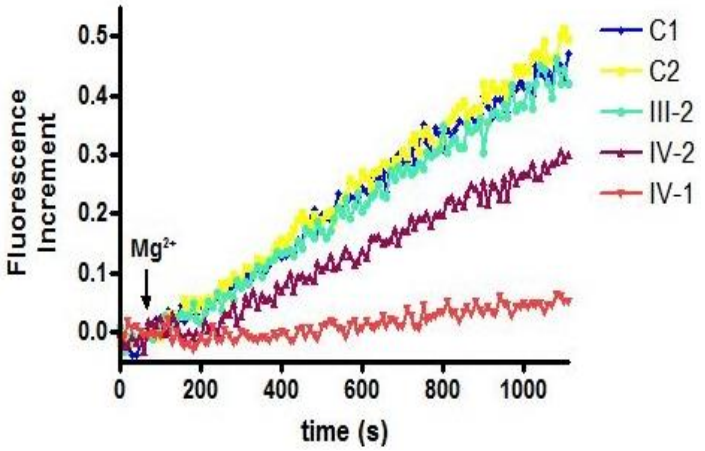

C.

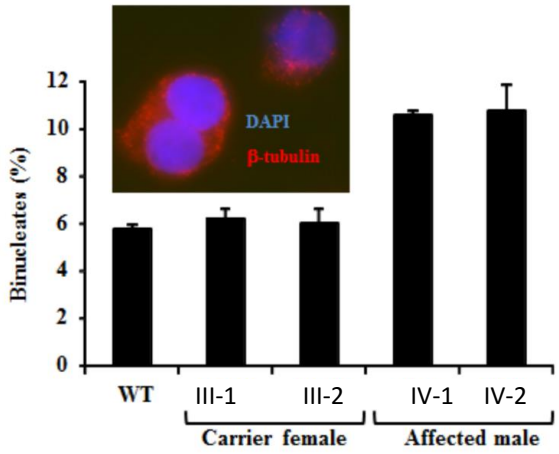

D.

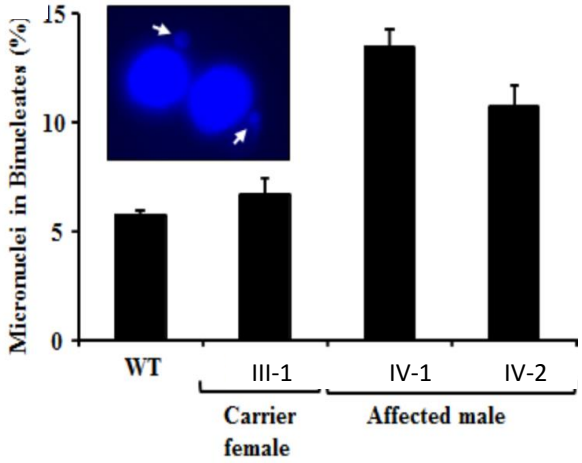

F.

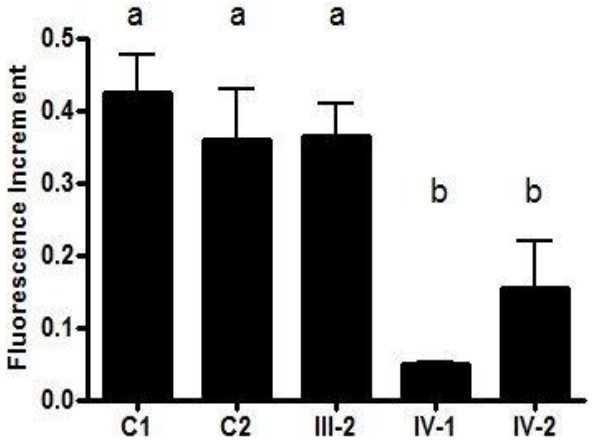

Supplementary Materials

1. Subjects

The family was ascertained for ID and dysmorphic features identified in the proband (IV-1), his two male cousins (IV-2 and IV-3, through his maternal aunt), his mother's male cousin (III-3, through her maternal aunt), and an affected but previously deceased great uncle (II-2) (Supplementary Figure 1). Individuals available and consenting to studies included 4/5 affected males, one unaffected male and 5 unaffected carrier females from 4 generations. Ethics approval was obtained from the UBC Clinical Research Ethics Committee.

2 Array CGH analysis

Array CGH analysis: Genomic DNA was extracted from peripheral blood using PUREGENE DNA Isolation Kits (Gentra, Minneapolis, MN). Diploid male and female reference DNA (Promega, Madison, WI) was used as controls. Whole genome array analysis using Agilent 105K oligonucleotide array-CGH was performed according to the protocol provided by the company (version 4.0, June 2006, Agilent Technologies, CA, USA) and reported previously [Fan et al., 2007; Qiao et al., 2010]. Commercial whole genome array Signature oligo array (SignatureChipOSTM) analysis was performed by Signature Genomics (Houston, Texas). High resolution whole genome Affymetrix 2.7M array and whole genome 105k oligo array was performed as previously described [Qiao et al., 2013]. Chromosome X array analysis was performed using Oxford Gene Technology CytoSure Chromosome X Array (Oxford Gene Technology, Begbrooke, UK). This high-density array has 44,000 features all focused on the X chromosome. Copy number/data analysis was performed with OGT's CytoSure™ /Oligome viewer software package which uses modified Circular Binary Segmentation to separate the data into regions of similar copy number.

[Venkatraman and Olshen, 2007]. Segments are called when at least 4 probes and the log2 ratio value is over 0.5.

Follow-up of whole genome array-CGH results: Fluorescent in situ hybridization (FISH) was performed using DNA probes from the CNVs detected in the patients. A Quantitative Multiplex PCR of Short fluorescent Fragments (QMPFS-PCR) assay was used as previously described [Charbonnier et al., 2000; Rajcan-Separovic et al., 2010] to assess the copy number status of Xp22.31 using primers for PNPLA4 gene on Exon 3 (Forward 5' TTG CCG AAG AAA TCA GAA GG 3' and Reverse 5' ATG CTG AGC TTG CCA AAG TT 3'). Primers designed from eleven genes from other chromosomes (available on request) served as normal copy number control genes. Gene deletion or duplication was considered when a 35-50% variation of the relative peak area of gene-specific sequences compared to those from a control pool was obtained after normalization.

3. X-chromosome inactivation: was performed by assaying methylation at the Androgen Receptor (AR) [Allen et al., 1992] locus using a PCR based protocol as detailed previously [Beever et al., 2003]. X-chromosome inactivation was expressed in terms of the percent inactivation of the smaller AR allele.

4. Haplotype analysis: Genotyping of 8 highly polymorphic markers spanning chromosome X was performed to determine the haplotypes segregating in this family. Markers typed (and their respective chromosome and genomic positions in hg 18) included DXYS233 (XpYp 0.8Mb), DXS6814 (Xp22.33 and Y, 1.3Mb), DXS1003 (Xp11.3, 46.4Mb), DXS6941 (Xp11.3, 48.2Mb), AR (Xq11.2, 66.7-66.8Mb), DXS1222 (Xq21.31, 87.3Mb), DXS1217 (Xq21.31, 88.2Mb) and, DXS1107 (Xq27.1 and Y, ~140Mb based on proximity to *SOX3*). PCR amplification was performed on a thermocycler with 35 cycles of 30s at 95C for denaturation, 45s at 55C for annealing, and 90s at 72C for elongation. The PCR products were

then visualized by automated fluorescence analysis using Applied Biosystems ABI Prism 310 genetic analyzer and GeneScan Analysis software.

5. Chromosome X exome sequencing

5.1 RainDance oligo library design

We obtained the target sequence for the human X-chromosome exome from the UCSC genome browser RefSeq Genes track (hg18). The total targeted sequence consisted of 7,427 fragments with a total size of 2,495,062 bases and included all coding and non-coding (3' and 5' untranslated regions) exons of human chromosome X. Oligo library design targeting this sequence for the RainDance micro droplet based enrichment is described in detail in Mondal et al, [Mondal et al., 2011; Mondal et al., 2012]. The final human X-chromosome exome RDT expanded content primer library consisted of 11,576 amplicons. The full length of DNA amplified was predicted to be 5,916,297 bases. In total, 98.05% of the targeted human X-chromosome exome bases (2,446,304 out of 2,495,062) were covered by at least one amplicon.

5.2 Enrichment of the targeted region by RainDance

Genomic DNA samples from two of the affected individuals, IV-2 and IV-3, were fragmented and processed in the RainDance instrument as described in Mondal et al, [Mondal et al., 2011].

5.3 Illumina library prep and sequencing

The sheared fragments from RainDance library were then purified using Qiagen QIAquick PCR purification column and was eluted in 32 µl of elution buffer. The samples then entered the standard Illumina multiplex library preparation protocol. At the enrichment step, a 6 base index tag was attached to each sample using PCR following the standard Illumina protocol. The only exception was that while purifying the adaptor-ligated products, we used Invitrogen E-Gel SizeSelect 2% (Invitrogen, catalogue #

G6610-02) instead of using the gel purification method suggested by Illumina. The enrichment was confirmed by running an Agilent BioAnalyzer 7500 DNA chip. A quantitative qPCR was done to quantify the library using KAPA Library quantification kit (KAPABiosystems, Woburn, MA, USA, catalogue # KK4824). Enriched DNA was denatured and cluster generation and multiplex 100bp paired-end sequencing (2 samples/lane) was performed using standard HiSeq protocol and as described in Bentley et al [Bentley et al., 2008].

5.4 Analysis of Illumina Sequencing Data

We mapped raw sequence data against a human X-chromosome exome reference sequence (hg18) consisting of 5,748 fragments with a total size of 4,723,733 bp. We used PEMapper (Cutler et al, in review) to map and identify variant sites, which included single nucleotide variants (SNVs) and insertions and deletions (indels). Variant sites were functionally annotated using SeqAnt [Shetty et al., 2010]. For each variant site, SeqAnt reports its type, functional classification (nonsense, replacement, silent, 5' or 3' UTR, intronic, intergenic), presence in databases like dbSNP, and evolutionary conservation (PhyloP, PhastCons). We then filtered variants with a custom perl script (blat_snp.pl) to identify the subset of variants that mapped to unique genomic regions. This script first obtains a test sequence that includes 25 bases upstream, the variant site, and 25 bases downstream. Each test sequence is then aligned against the entire human genome using UCSC BLAT [Dreszer et al., 2012] to determine the number of times it is found in the human genome. We retained variants that mapped uniquely to the human genome (BLAT = 1) for subsequent analyses. We used the following filter criteria to identify putative mutations: 1) variants which were novel (i.e. not present in dbSNP132), 2) variants present in both the sequenced cases (IV-2 and IV-3), 3) variants that fell within the haplotype block (chrX: 46,319,301-140,000,000) and 4) variants at a site with high conservation score (placental Phastcons>0.8). As shown in Supplementary Table 3, out of the total 1109 total variants, 153 were novel, while the remaining 956 were already catalogued in dbSNP132. Of the 153 novel variants, a total of 7 were called in both IV-2 and IV-3, and 6 of these were found within the previously mapped haplotype block. Of these

six variants, only four were found at sites with a high Phastcons score (> 0.8) and are shown in Supplementary Table 4. We assumed that the exonic silent (ChrX:106,003,539) variant was unlikely to be a mutation, and followed up the remaining 3 exonic variants [*ATRX* (p.G2465Vfs*15), *ATG4A* (p.N234K), *TENM1* (p.H2185L)].

5.5 Validation of candidate variants

Sanger sequencing was used to confirm the segregation of candidate variants with the phenotype. The PCR primers used for validation are listed in Supplemental Table 1 and were designed using Primer3Plus (http://www.bioinformatics.nl/cgi-bin/primer3plus/primer3plus.cgi). Amplicons with the expected size were then purified using either Centrifugal units (Millipore, USA) or Wizard SV gel and PCR cleanup system (Promega, USA), when the PCR reaction contained single or multiple bands respectively.

6. Functional analysis

6.1 RNA expression: Total RNA was extracted from the EBV-transformed patient-derived lymphoblast cell lines (LCL) using an RNeasy Plus Mini kit (Qiagen). Aliquots (~500ng) of the total RNA extracts prepared from the LCL cultures were subsequently reverse-transcribed into cDNA using GeneAmp Gold RNA PCR Core Kit (Applied Biosysterm). The presence of isoforms in MAGT1 was tested by RT-PCR using primers for exon 1, 5 and 8 (Exon1-8: Forward 5'-GAAGGGAGAGGAGCGAACAT-3', Reverse 5' CAAGTCCAATAC CAGCCACA-3'; Exon1-5: Forward 5'-GAAGGGAGAGGAGCGAACAT-3', Reverse 5'-CAACATAAGGGGACCAGCAT-3')

6.2 Real-time quantitative (q)RT-PCR: The first-strand cDNA generated from the LCLs served as a template for qRT-PCR using the ABI PRISM 7300 Sequence Detection System (Perkin-Elmer Applied

Biosystems) equipped with a 96-well optical reaction plate for primers specific for *ATRX, MAGT1, ATG4A* or the housekeeping gene, β-actin. The specific nucleotides sequences for these primers are as follows:

ATRX (Exon 35) Forward 5'- AGAAG GCTCC AGCAG CAGTA -3', Reverse 5'- CTGGC TGATA CATTC CTCTC A -3'; *MAGT1* (Exon 3) Forward 5'- GCAAG CTGAT GAAGA ATTCC A -3', Reverse 5'- GCCTT CATCA AAATC CACCA -3'; *ATG4A* (Exon 7-8) Forward 5'- GAATG GAATT CCTTG GCTGT -3', Reverse 5'- GCAGA GGTGC CCTTA CTCTG -3'; β-actin (Exon3-4) Forward 5'- CATCG AGCAC GGCAT CGTCA -3', Reverse 5'-TAGCA CAGCC TGGAT AGCAA C -3' .

Real-time qPCR was performed using SYBR® Green PCR Master Mix (Applied Biological Materials Inc, Richmond, BC). The amplification efficiency was determined by plotting log cDNA dilution against ΔCT (ΔCT =CT.Target-CT.Actin), with acceptable efficiency of 90-110%. ΔΔCT was determined using the formula ΔΔCT= (CT Target-Ct.Actin) Patient - (CT.target-CT Actin) Control. All PCR reactions were performed in triplicate, with the mean of $2^{-\Delta\Delta CT}$ values being used to determine mRNA levels for each subject. Relative ATRX, MAGT1 and ATG4A mRNA levels for the patient and control groups were obtained by calculating the average of $2^{-\Delta\Delta C}$ values for patients as a group and controls as a group, and determining the difference between the group averages using the Student's t test (VassarStat Statistical Computation website). Data were analyzed using SDS 2.0 software (Applied Biosystems). In addition, one-way analysis of variance (ANOVA) was used to analyze significant differences among individuals by GraphPad Prism 4 computer software; $p<0.05$ was considered significant.

6.3 Western blotting: LCLs were washed three times in PBS and incubated in 1mL RIPA buffer (Thermo Scientific, USA), supplemented with Halt Phosphatase Inhibitor Cocktail (Thermo Scientific, USA) for 15 minutes on ice. Cell lysates were centrifuged at 10,000 x g for 15 minutes at 4°C, and the supernatants were used for Western blotting. Cell lysate protein concentrations were determined using a

DCTM Protein Assay (BioRad laboratories, USA). Western blots containing cell-lysate aliquots (~30 µg) were prepared and immunoblotted using a polyclonal antibody directed against human MAGT1 (17430-1-AP Proteintech Group, Inc. IL, USA), ATRX (NBP1-32851, NovusBiologicals, Littleton, USA) or ATG4A (83290, Abcam, Toronto). To standardize the amounts of protein loaded into each lane, the blots were either reprobed with a monoclonal antibody directed against human β-actin (NovusBiologicals, Littleton, USA), or cut in half with the upper half membrane been probed with ATRX, and the lower half probed with β-actin. The ECL Western Blotting system was used to detect the amount of each antibody bound to antigen and the resultant photographic films were analyzed by UV densitometry (GE Healthcare Life Sciences, Pittsburgh, USA). The absorbance values obtained for MAGT1 and ATRX were then normalized relative to the corresponding β-actin absorbance value. The average of MAGT1 and ATRX protein expression was obtained from three independent replicates from the subject and the control samples.

6.4 Magnesium influx measurements: For each sample 2×10^6 LCL cells were incubated with the Mg^{2+}-sensitive fluorescent dye Mag-Fluo-4-AM (Invitrogen) (1 µM) for 20 minutes at 37°C in loading buffer (LB) containing: 120 mM NaCl, 20mM HEPES, 4.7mM KCl, 1.2mM KH_2PO_4, 1.2 mM $CaCl_2$, 1.2 mM $MgCl_2$, 10mM glucose, pH 7.4. Immediately before use, the Mag-Fluo-4-AM stock solution was mixed with a 20% (w/v) Pluronic F-127 stock solution in DMSO (Invitrogen) at a ratio 1:1, to help disperse the AM form of the indicator in LB. At the end of the incubation, Mag-Fluo-4-loaded cells were washed once in LB and then suspended in influx buffer (IB) containing: 120 mM N-methyl-D-glucamine, 20mM HEPES, 4.7mM KCl, 1.2mM KH_2PO_4, 10mM glucose, pH 7.4. Fluorescence emission of Mag-Fluo-4-loaded cells was monitored at 517 nm with a SPEX Fluoromax spectrofluorometer (excitation wavelength 488 nm) with a time increment of 10 s and an integration time of 10 s. Fluorescence measurements were carried out at 37°C with continuous stirring of cell suspensions for 15 minutes. Baseline was recorded for 2 minutes and then 1 mM $MgSO_4$ was added. Signal intensity is reported as the fluorescence increment $\mu F=F/F_0$, where F is the fluorescence measured at a given time and F_0 is the mean

baseline fluorescence. Statistical analysis was carried out using GraphPad Prism 4 software; a p value <0.05 was considered significant. The difference between the group averages of controls and patients was evaluated by Student t test. Comparison between individuals was performed using ANOVA followed by Newman-Keuls multiple comparison test.

6.5 Quantification of DNA methylation: 300 ng of genomic DNA was bisulfite converted using the EZ DNA Methylation Gold Kit (Zymo Research, Orange, CA, USA) following manufacturer's protocol. A set of PCR primers was designed to amplify the CpG-rich rDNA promoter based on the sequence in Fig 1A of Uemura et al, [Uemura et al., 2012]. Each PCR product was subsequently pyrosequenced using a PyroMark MD system (Biotage, Uppsala, Sweden) with three different sequencing primers. The level of DNA methylation was quantified at 26 CpG sites and a standard error of the mean was calculated within each group (carriers n=5, affected n=4 and negative controls n=25) (Supplementary Figure 2). DNA methylation across the 26 CpG sites was highly correlated (Spearman rank order correlation), and thus methylation was averaged across all sites in the rDNA promoter for each individual. As DNA methylation was not significantly different between male and female controls on average or at any individual CpG (Mann-Whitney test), both males and females were included in the control group. Neither average rDNA methylation nor individual CpG methylation was correlated with XCI in female controls (Spearman rank order correlation). Mann-Whitney tests, followed by Bonferroni correction was performed to determine whether average rDNA promoter methylation differed between affected and controls or carriers and controls. The design of sequencing primers for assessment of rDNA promoter methylation is shown in Supplementary Figure 6.

6.6 Cell cycle defects:

a) Immunofluorescence: Asynchronously growing LCLs were harvested, swollen in 75mM KCL (10mins), fixed in 3.7% paraformaldehyde (10 mins) and cytospun (CytoSpin, Shandon) on poly-L-lysine coated slides. Samples were permeabilized using Triton X-100 (0.1% in 5% BSA-PBS), blocked using

5% BSA-PBS (10 mins) and stained for 30 mins using anti-β-tubulin primary antibody (H-235 from Santa Cruz), counterstained with anti-rabbit Cy3 secondary antibody (DAKO), before staining the nuclei with DAPI. Slides were analysed using the Zeiss AxioPlan platform and images captured using SimplePCI software.

b) Micronuclei in binucleate cells: Micronuclei were visualized in cytochalasin B-induced binucleate cells (1.5µg 24hrs) using DAPI staining as described above.

References

Allen RC, Zoghbi HY, Moseley AB, Rosenblatt HM, Belmont JW. 1992. Methylation of HpaII and HhaI sites near the polymorphic CAG repeat in the human androgen-receptor gene correlates with X chromosome inactivation. Am J Hum Genet 51:1229-39.

Beever CL, Stephenson MD, Penaherrera MS, Jiang RH, Kalousek DK, Hayden M, Field L, Brown CJ, Robinson WP. 2003. Skewed X-chromosome inactivation is associated with trisomy in women ascertained on the basis of recurrent spontaneous abortion or chromosomally abnormal pregnancies. Am J Hum Genet 72:399-407.

Bentley DR, Balasubramanian S, Swerdlow HP, Smith GP, Milton J, Brown CG, Hall KP, Evers DJ, Barnes CL, Bignell HR, Boutell JM, Bryant J, et al. 2008. Accurate whole human genome sequencing using reversible terminator chemistry. Nature 456:53-9.

Charbonnier F, Raux G, Wang Q, Drouot N, Cordier F, Limacher JM, Saurin JC, Puisieux A, Olschwang S, Frebourg T. 2000. Detection of exon deletions and duplications of the mismatch repair genes in hereditary nonpolyposis colorectal cancer families using multiplex polymerase chain reaction of short fluorescent fragments. Cancer Res 60:2760-3.

Dreszer TR, Karolchik D, Zweig AS, Hinrichs AS, Raney BJ, Kuhn RM, Meyer LR, Wong M, Sloan CA, Rosenbloom KR, Roe G, Rhead B, et al. 2012. The UCSC Genome Browser database: extensions and updates 2011. Nucleic Acids Res 40:D918-23.

Fan YS, Jayakar P, Zhu H, Barbouth D, Sacharow S, Morales A, Carver V, Benke P, Mundy P, Elsas LJ. 2007. Detection of pathogenic gene copy number variations in patients with mental retardation by genomewide oligonucleotide array comparative genomic hybridization. Hum Mutat 28:1124-32.

Mondal K, Ramachandran D, Patel VC, Hagen KR, Bose P, Cutler DJ, Zwick ME. 2012. Excess variants in AFF2 detected by massively parallel sequencing of males with autism spectrum disorder. Hum Mol Genet 21:4356-64.

Mondal K, Shetty AC, Patel V, Cutler DJ, Zwick ME. 2011. Targeted sequencing of the human X chromosome exome. Genomics 98:260-5.

Qiao Y, Harvard C, Tyson C, Liu X, Fawcett C, Pavlidis P, Holden JJ, Lewis ME, Rajcan-Separovic E. 2010. Outcome of array CGH analysis for 255 subjects with intellectual disability and search for candidate genes using bioinformatics. Hum Genet 128:179-94.

Qiao Y, Tyson C, Hrynchak M, Lopez-Rangel E, Hildebrand J, Martell S, Fawcett C, Kasmara L, Calli K, Harvard C, Liu X, Holden JJ, et al. 2013. Clinical application of 2.7M Cytogenetics array for CNV detection in subjects with idiopathic autism and/or intellectual disability. Clin Genet 83:145-54.

Rajcan-Separovic E, Diego-Alvarez D, Robinson WP, Tyson C, Qiao Y, Harvard C, Fawcett C, Kalousek D, Philipp T, Somerville MJ, Stephenson MD. 2010. Identification of copy number variants in miscarriages from couples with idiopathic recurrent pregnancy loss. Hum Reprod 25:2913-22.

Shetty AC, Athri P, Mondal K, Horner VL, Steinberg KM, Patel V, Caspary T, Cutler DJ, Zwick ME. 2010. SeqAnt: a web service to rapidly identify and annotate DNA sequence variations. BMC Bioinformatics 11:471.

Uemura M, Zheng Q, Koh CM, Nelson WG, Yegnasubramanian S, De Marzo AM. 2012. Overexpression of ribosomal RNA in prostate cancer is common but not linked to rDNA promoter hypomethylation. Oncogene 31:1254-63.

Venkatraman ES, Olshen AB. 2007. A faster circular binary segmentation algorithm for the analysis of array CGH data. Bioinformatics 23:657-63.

Supplementary Figure 1

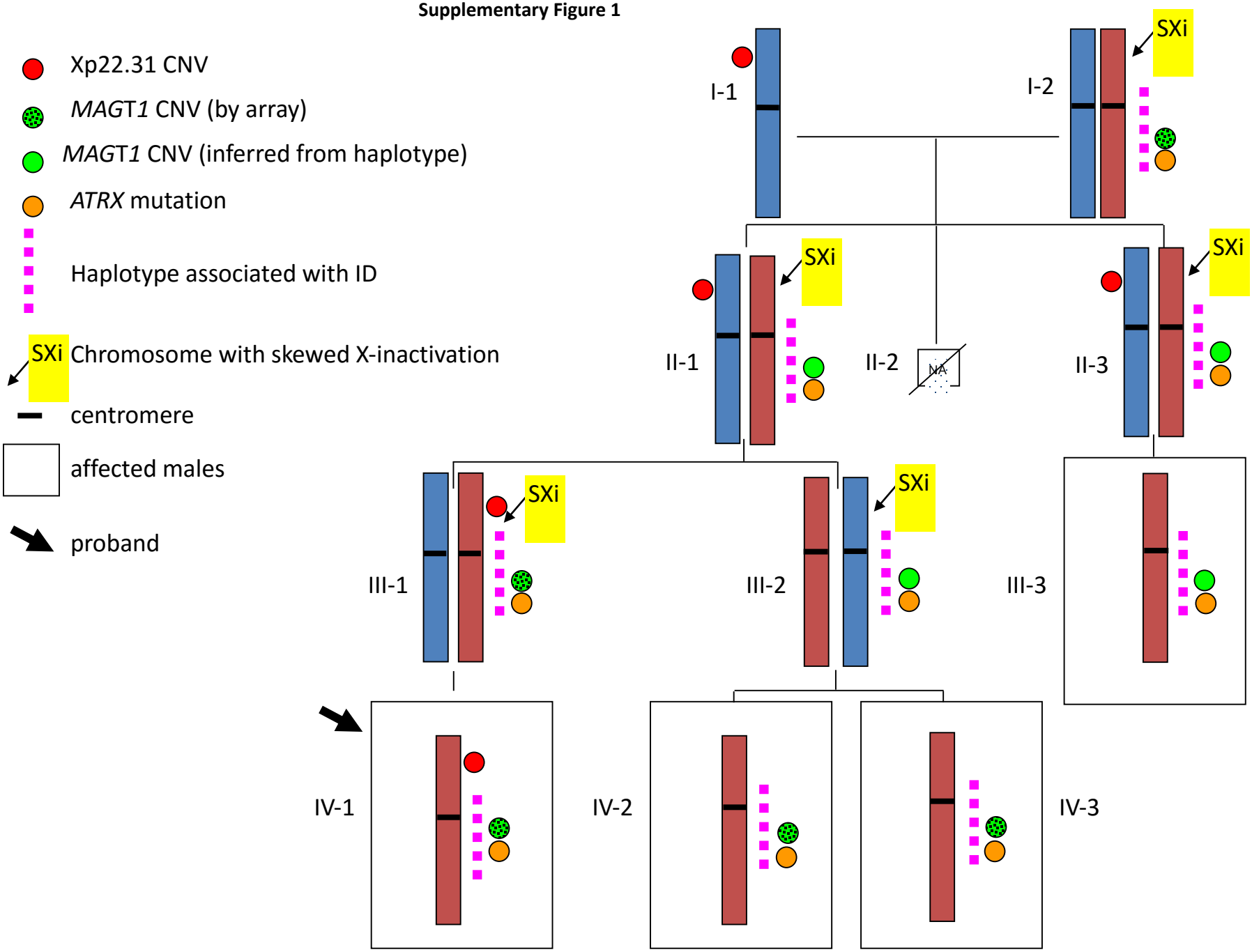

Supplementary Figure 1. Family tree and summary of genetic findings.

Supplementary Figure 2

A.

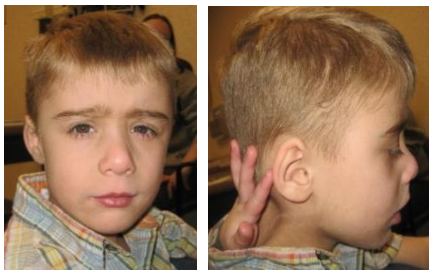

a b

B.

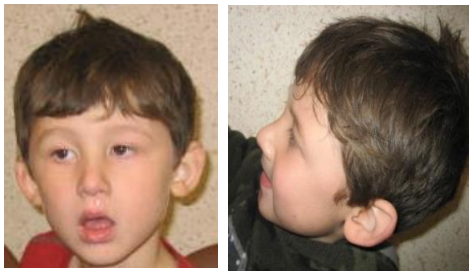

a b

C.

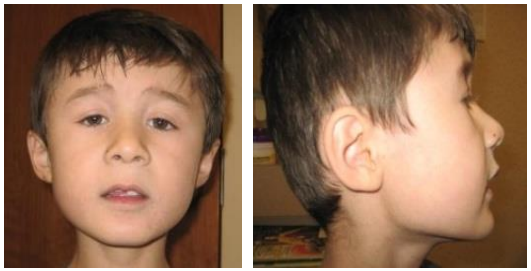

a b

D.

a b c d e f g h

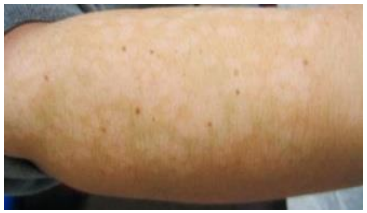

i

Supplementary Figure 2. Clinical features. Facial features and prominent low set ears in IV-1 (Aa and Ab), IV-2 (Ba and Bb) and IV-3 (Ca and Cb). D) Skin and nail appearance. Curved toe nails in IV-1 (a) and IV-3 (b). Crinkly palm skin in IV-1 (c) and IV-3 (d). Crinkly skin on hands and soles of IV-3 (e and f). Grooved nails in IV-1 (g) and his mother III-1 (h). Pigmented forearm skin in III-1 (i).

Supplementary Figure 3

A.

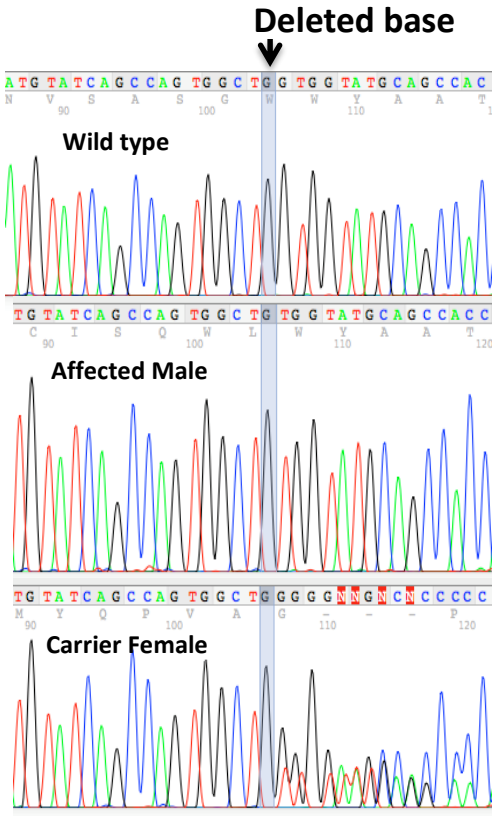

B.

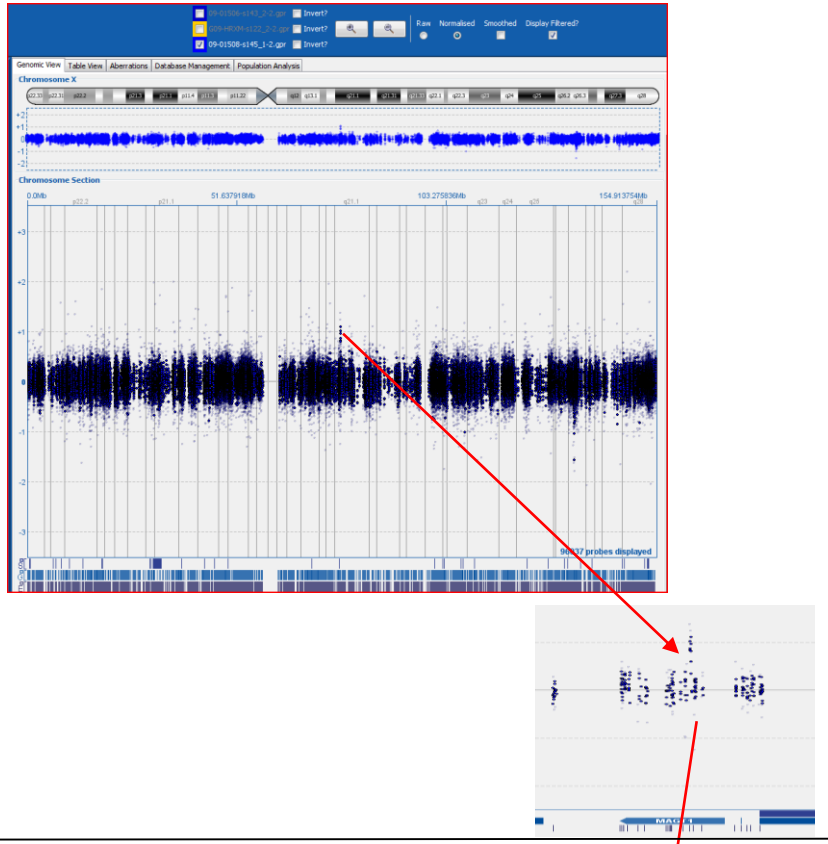

C.

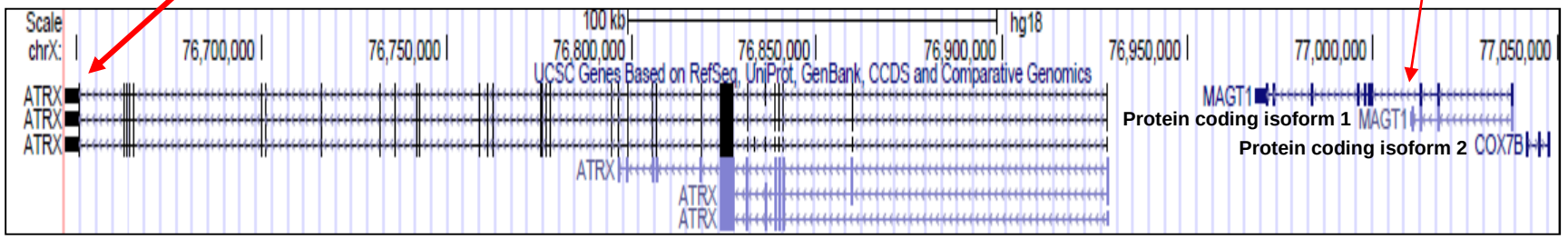

D.

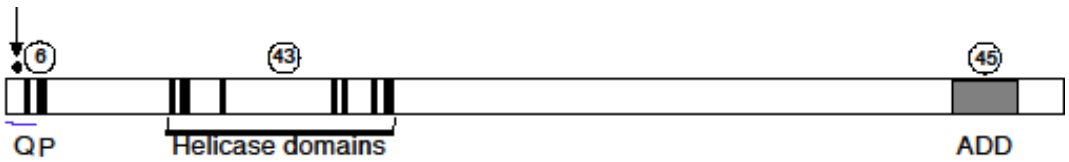

Supplementary Figure 3. *ATRX* and *MAGT1* mutations. a) Single nucleotide deletion in *ATRX*. b) Chromosome X array with *MAGT1* CNV (enlarged in inset). c) Position of *ATRX* single nucleotide deletion in exon 36 and *MAGT1* CNV in intron 3 which contains an alternative splice site and overlaps 3'UTR of isoform 2, UCSC, hg18. d) Schematic diagram of the *ATRX* gene (not to scale). The blue horizontal line represents exon 36. The mutation discovered in this study is indicated with an arrow. The principal domains, the zinc finger motif (ADD) and the highly conserved helicase motif, are indicated as are the conserved P box (P) and a glutamine-rich region (Q). Total number of mutations in ADD, helicase and the C terminus is indicated by numbers inside circles. A total of 6 different constitutional mutations have previously been reported near the C-terminus of *ATRX*, all of which lead to protein truncation [Gibbons et al., 2008].

Supplementary Figure 4

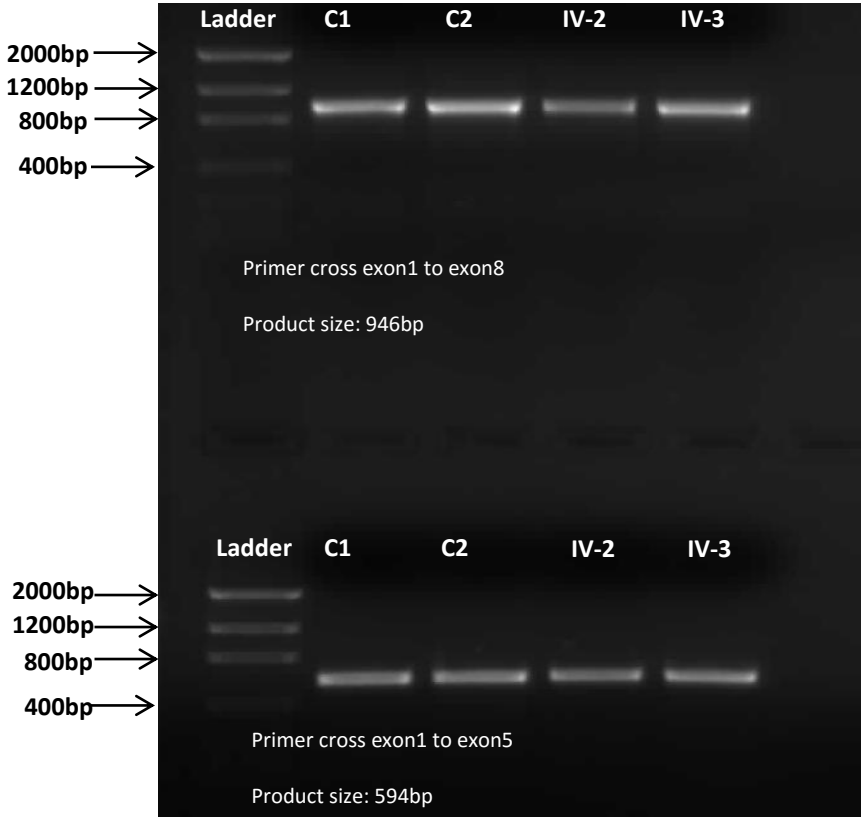

Supplementary Figure 4: RT-PCR products for *MAGT1* gene. C1 and C2 are controls.

Supplementary Figure 5

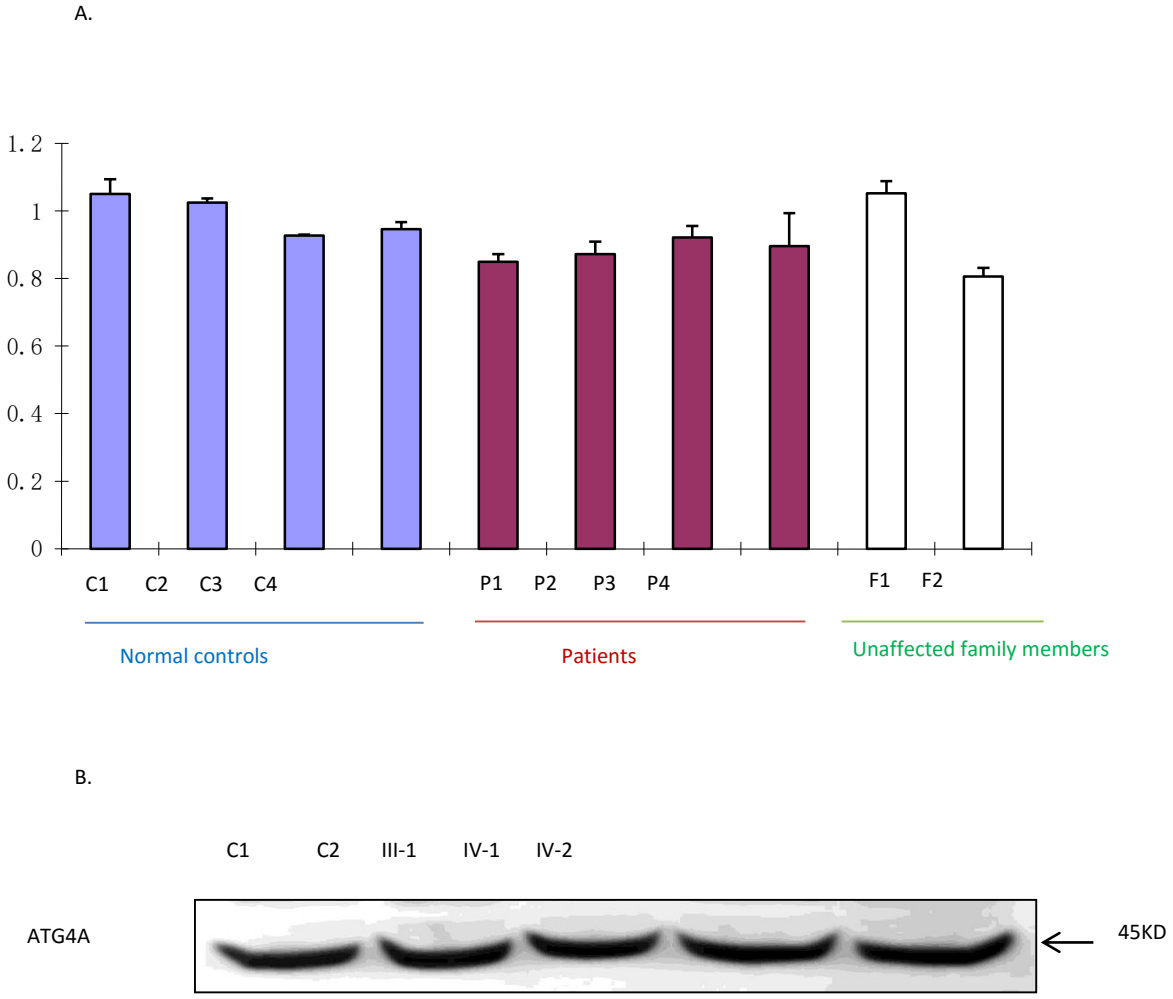

Supplementary Figure 5: *ATG4* RNA(a) and protein(b) expression. C= controls.

Supplementary Figure 6

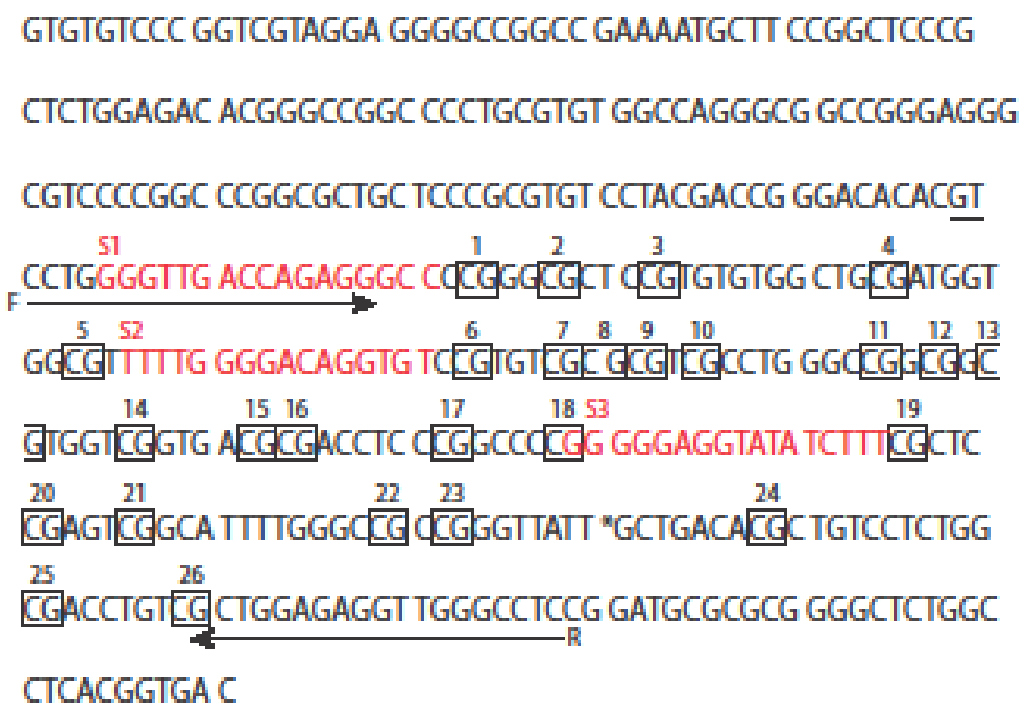

Primers

F	5' - GTT TTG GGG TTG AAT AGA GG - 3'
R	5' - biotin – AA AAC CCA ACC TCT CCA AC - 3'
S1	5' - GGG TTG ATT AGA GGG TT - 3'
S2	5' - TTT TGG GGA TAG GTG T- 3'
S3	5' - GGG GGA GGT ATA TTT TT - 3'

Supplementary Figure 6: Primer design for rDNA methylation analysis.

Supplementary table 1. Summary of clinical findings.

	IV-1	**IV-2**	**IV-2 second visit**	**IV-3**	**II-2 (deceased)**	**III-3**	**I-2**	**III-1**
Age at assessment	5Y 9M	7Y 3M	8Y 3M	6Y 7M	died at 40 years due to chronic progressive pulmonary condition			
DD	Y	Y	Y	Y	very delayed, lived in special care facility	very delayed		
Growth	short stature (consistently well below the 3rd centile at 5-6 SD below respective height and weight means)	thin	thin	not gaining waight	thin from late childhood, short	thin from late childhood , short		
Cranium	tall forehead	normal		normal				
Face	hypertelorism; flat facial profile, broad, thick eyebrows with partial synophrys, hypertelorism, bilateral epicanthus inversus, short palpebral fissures, thickened scaphahelices of the ears and broad nasal root and bridge	Broader superiorly and narrower inferiorly with somewhat squared mandibular tip, telecanthus, possible hypertelorism .	rounded inverted triangle shape, malar hypoplasia, facial hypotonia	rounded inverted triangle shape, malar hypoplasia.	not like younger males	not like younger males		

Ears/hearing	Otitis media-recurrent, pressure-equalization tubes. Exteranl normal	mildly coarse, low-set; possible hearing loss; tube placemnet at 4 years of age	pressure-equalization tubes, auricles get read and inflamed and hot, ears lowset, somewhat prominient	Pressure-equalization tubes; auricles get red and inflamed and hot, and they scratch at it. External-normal to lowset, rather prominent.				
Eyes/vision	won't look into your eyes for more than a second. Had corrective stents inserted for blocked tear ducts	palpebral fissures-short and downslanting, brows raised medially in somewhat of an inverted 'swoosh' shape, suggestion of ptosis. sclerae-normal, conjuntivae-clear, irises-normal, pupils-round and regular.	short, downslanting palpebral fissures, highly-arched eyebrows.	short, downslanting palpebral fissures, highly-arched eyebrows.				
Nose	Tip-small, tip-unturned	Prominent nasal bridge that flares superiorly, mild hypoplasia of nasal alae and blunting of nasolabial	constant runny nose	Constant runny nose. Unremarkable shape.				

		angles. philtrum-long						
Mouth	Mouth normal, tongue deeper midline grove	Microstomia, upper lip-thin.	oral surgery for molars, caps, unusual swallowing-pushes tongue back to swallow	Oral surgery for molars, caps, microstomia				
Neck	long, right submandibular auricular lymphadenopathy	thin						
Extremities	Transverse palmar crease on right, palms and soles are soft, pillowy, with increased fine creases, digits generally well formed. Normal fingernails, toenails are grooved, cracked, concave	clinodactily-bilateral 5th finger, foot sandal gap	nails dysplastic, thin, wavy and longitudinally grooved nails	dysplastic, thin, wavy and longitudinally grooved nails.			grooved thumbnail	grooved thumbnail
Skin abnormality	Pruritus, not as bad as cousins, and worse after a bath. Does not usually break skin. Also has **crinkly skin always,** like it's water logged, on hands and feet. Mild generalized hyperpigmentation, no clear depigmented areas even under Woods lamp exam. One tiny linear area on upper mid abdomen that looks like an old scar but could be hypopigmented macule.	history of eczema, integument photosenzitivty, **markedly crinkly but soft skin** on his palms and soles, some thickening and excessive creasing on dorsum; mild hirsutism; areas of indistinct **blotchy**	infections due to skin picking and scratching and reduced sensation of pain, persistent pruritus and soft, crepe paper-like hyperkeratosis of palms and soles, temperature instability with	He has pruritus and hyperkeratosis of palms and soles. He has some temperature instability and some **variable blotchyness** or **flushing on face**, ears, extremities. Color changes in hands, feet,	hyperkeratosis of palms and soles; marked decrease in senzitivity to pain, temperature and **cutaneous flushing**	marked decrease in senzitivity to pain, temperature and **cutaneous flushing**		right forearm and right lower chest has spotty depigmentatai on; pruritus on right lower chest

	Observed to scratch arms	**brown-purple to reddish** mottling around lower legs and ankles; numerous small post-excoriation scars (well healed) on anterior chest. Also has blotchy skin on his shins and around his ankles. He has generalized pruritus, causing scratching with bleeding even when an area of irritated skin is not present.	**variable blotchiness or flushing on face**, ears and extremities, hive like changes	face-blotchy, hive like changes. Takes a long time to heal skin. Excess scratches improved but still present; crepe paper like hyperkeratosis of palms and soles.				
GI	chronic constipation controlled on miralax qd		constipation					
Neurology/behaviour	ASD, severe ID, stereotypy of spinning objects and becoming over focused on that activity. Neurologic mental status:oriented, Interaction: juvenile for age, communication:none.cranial nerves-III through	ID, ADHD combined type, past history of autism; hyperactive with limited eye contact and cooperation,	Overexcited around new people, jaw clinching. Hyperactive, socially engaged but in distant manner, not potty trained	ID, Overexcited around new people, jaw clinching. Hyperactive, socially engaged but in distant	ID	ID	No developmental deficit	No developmental deficit

	XII grossly normal, DTRs symmetric, 0+ - 1+. not toilette trained, mild seizures	interaction-juvenile for age, communicatio n-limited. muscle tone-normal, history of seizures temporaly related to shots at 4m of age		manner, not potty trained				
Speech delay	no verbal communication, except stereotypic cries and screems. Severe expressive language delay	communicatio n-limited. Severe expressive language delay	limited speech quick and short, sometimes difficult to understand. Severe expressive language delay	Communicati on problems. limited speech quick and short, sometimes difficult to understand. Severe expressive language delay				
Musculoskeletal	muscle tone normal to decreased, muscle mass normal		loose joints, poor muscle tone, facial hypotonia	loose joints, poor muscle tone,	joint limitation	joint limitation		

Notes: ASD: autism spectrum disorder. DTR: Deep Tendon Reflexes. ADHD: Attention deficit hyperactivity disorder. Qd: quaque die (every day).

Supplementary Table 2: Summary of genetic investigations

Subject	Whole genome	FISH confirmation	chromosome X specific array	Breakpoints	Size	Gene content	QMPSF for Xp22.31	Skewed X inactivation
IV-1	dup Xp22.31*	CTD-2052I13 inconclusive	dup Xp22.31	Xp:6,467,401- 8,091,811;	1.6Mb	*HDH1A, VCX, PNLPA4, STS*	NA	NA
			dup Xq21.1	Xq:77,009,644-77,010,488	0.8kb	*MAGT1*	NA	
	del 11p15.1*	RP11-118A del	NA	11p:18,994,447-19,849,379	0.85Mb	*ZDHHC13, CSRP3, MRGPRX2, NAV2, E2F8*	NA	
IV-2	normal#,§	NA	dup Xq21.1	Xq:77,009,644-77,010,488	0.8kb	*MAGT1*	absent	NA
IV-3	normal#	NA	dup Xq21.1	Xq:77,009,644-77,010,488	0.8kb	*MAGT1*	absent	NA
III-1	dup Xp22.31*	NA	dup Xp22.31	Xp:6,467,401- 8,091,811	1.6Mb	*HDH1A, VCX, PNLPA4, STS*	NA	yes
			dup Xq21.1	Xq:77,009,644-77,010,488	0.8kb	*MAGT1*	NA	
III-2	normal§	NA	NA	NA	NA	NA	absent	yes
III-3	normal§	NA	NA	NA	NA	NA	NA	NA
II-1	NA	NA	NA	NA	NA	NA	present	yes
II-2	NA	NA	NA	NA	NA	NA	present	yes
I-2	NA	NA	dupXq21.1	Xq:77,009,644-77,010,488		*MAGT1*	absent	yes
I-1	Xp22.31dup&	NA	NA	Xp:6,498,521-8,091,951	NA	NA	NA	NA

Array type: * Signature; # OGT whole genome; § Affymetrix 2.7M array. NA: not analyzed

Supplementary Table 3: Analysis of genetic variants detected by exome sequencing.

Total variants called in IV-2 and IV-3	1109
Variants in dbSNP132	956
Criteria 1: Novel variants (not in dbSNP 132)	153
Criteria 2: Variants called in both IV-2 and IV-3 only	7
Criteria 3:Variants within the haplotype block (ChrX: 46,319,301-140,000,000)	6
Criteria 4: Variants with Placental Phastcons >0.8	4

Supplementary table 4: Candidate chromosome X variants.

Position (hg18)	Functional Classification	Variant Type	Placental PhastCons	Gene	Mutation	Validated
ChrX:76,650,570	Exonic Indel	Single base-pair Deletion, frameshift mutation	1	*ATRX*	p.G2465Vfs*15	Yes
ChrX:106,003,539	Exonic Silent	SNV	0.996	*TBC1D8B*	p.A1017A	ND
ChrX:107,267,844	Exonic Replacement	SNV	1	*ATG4A*	p.N234K	Yes
ChrX:123,345,887	Exonic Replacement	SNV	1	*TENM1*	p.H2185L	Yes

Supplementary table 5: primers used for Sanger sequencing.

Position	**Gene**	**Forward primer(5'-3')**	**Reverse primer(5'-3')**
chrX:76650570	*ATRX*	TTGGCATTTAAGGGGACCAAAC	CAATCAGCAGCAACAGCAACAA
chrX:107267844	*ATG4A*	GGCCCTGGCAGACTTGAGAA	CTGAGATGGCGGTGTGATGG
chrX:123345887	*TENM1*	GCTTTCTGCAGCAGGCCATT	AATGTGGGCCGCATGGTAAT